Immune effector monocyte–neutrophil cooperation induced by the primary tumor prevents metastatic progression of breast cancer

Catharina Hagerling[a,b,1,2], Hugo Gonzalez[a,3], Kiarash Salari[a,3], Chih-Yang Wang[a,4], Charlene Lin[a], Isabella Robles[a], Merel van Gogh[a], Annika Dejmek[c], Karin Jirström[b], and Zena Werb[a,d,2]

[a]Department of Anatomy, University of California, San Francisco, CA 94143-0452; [b]Department of Clinical Sciences, Division of Clinical Oncology and Pathology, Lund University, SE-221 85 Lund, Sweden; [c]Department of Translational Medicine, Lund University, Malmö SUS, SE-214 21 Malmö, Sweden; and [d]Helen Diller Family Comprehensive Cancer Center, University of California, San Francisco, CA 94143

Metastatic behavior varies significantly among breast cancers. Mechanisms explaining why the majority of breast cancer patients never develop metastatic outgrowth are largely lacking but could underlie the development of novel immunotherapeutic target molecules. Here we show interplay between nonmetastatic primary breast cancer and innate immune response, acting together to control metastatic progression. The primary tumor systemically recruits IFNγ-producing immune effector monocytes to the lung. IFNγ up-regulates *Tmem173/STING* in neutrophils and enhances their killing capacity. The immune effector monocytes and tumoricidal neutrophils target disseminated tumor cells in the lungs, preventing metastatic outgrowth. Importantly, our findings could underlie the development of immunotherapeutic target molecules that augment the function of immune effector monocytes and neutrophils.

metastatic breast cancer | immune effector monocytes | CCR2 | CCL2 | STING

Metastatic breast cancer is a major clinical challenge, accounting for a discouraging 400,000 deaths per year worldwide (1, 2). Importantly, metastatic behavior varies significantly among breast cancers with ~10 to 15% of breast cancer patients developing distant metastases (3). A wide range of tumor-derived and stromal factors has been shown to promote metastatic progression (2, 4). However, although the majority of breast cancer patients never develop metastatic breast cancer, it remains to be determined whether primary breast cancer tumors can actively induce a systemic antimetastatic immune response protecting patients from metastatic outgrowth, which could potentially provide the backbone for the future development of immunotherapeutic target molecules.

Cancer immunotherapy has proven to be a promising treatment, improving the survival of patients with cancer; however, currently there are no immunotherapies available for advanced breast cancer (5). In fact, the majority of current cancer immunotherapies primarily target or augment the function of T lymphocytes rather than myeloid cells, which have an important role in innate immunity and are critical regulators of metastatic breast cancer (5, 6). The main myeloid populations involved in metastatic breast cancer are mononuclear monocytes and macrophages, and polymorphonuclear neutrophils (7–9). Within each myeloid population there is a continuum of subpopulations that can have either a pro- or antitumoral phenotype (6, 7). Novel cancer immunotherapies that activate and augment the function of antitumoral myeloid subpopulations could have therapeutic potential and be clinically important for patients with advanced breast cancer.

Here we elucidate whether nonmetastatic primary human breast cancer can evoke an antimetastatic myeloid immune response at the metastatic site, explaining disparities in the development of metastatic breast cancer in patients. We took advantage of the difference in metastatic efficiency between various breast cancer patient-derived xenograft (PDX) lines (10, 11). The PDX model harbors bona fide malignancy characteristics directly from the

patients' breast cancer tumors and is hence an attractive preclinical model to find novel therapeutic alternatives for metastatic breast cancer (12). We furthermore validated our PDX-derived findings with a large primary breast cancer tissue microarray (TMA), pleural effusions from breast cancer patients and an immunocompetent syngeneic mammary cancer model. Taken together, we reveal interplay between the primary breast cancer tumor and myeloid immune response, acting together to control metastatic progression.

Results

Monocyte Recruitment in a Nonmetastatic Model. We studied 3 different triple negative breast cancer PDX lines that in prior work we found had high (PDX lines HCI-001 and HCI-010) or poor (PDX line HCI-002) spontaneous metastatic efficiency (Fig. 1 *A* and *B* and *SI Appendix*, Table S1) (11). Their metastatic behavior in mice recapitulated patterns similar to those observed in the original patients (11, 12). The PDX tumors were transplanted

orthotopically and allowed to grow to end point (∼20 to 25 mm in diameter) in nonobese diabetic (NOD)/severe combined immunodeficient (SCID) mice, which are deficient in mature T and B cells but can have functionally activated innate immune cells (13, 14). Accordingly, they provide an appropriate model to explore the direct impact of innate immune cells in human metastatic breast cancer.

To discern if the differences in the metastatic behavior of the PDXs were independent or dependent upon mechanisms intrinsic to the cancer cells we did a bilateral transplantation experiment (Fig. 1C). We asked if either a highly metastatic or a poorly metastatic PDX line could systemically modulate metastatic efficiency of the other PDX line. We used the HCI-001 line, which has similar primary tumor growth kinetics as HCI-002 but excluded the

HCI-010 line from the experiment since HCI-010 tumors grow slower (SI Appendix, Fig. S1A) (12). As expected, we did not detect any metastatic foci in lungs of HCI-002 tumor-bearing mice (transplanted to only 1 side), (Fig. 1D). Intriguingly, compared to HCI-001 tumor-bearing mice (transplanted to only 1 side), the number of metastatic foci in the lungs of HCI-001/HCI-002 tumor-bearing mice decreased (Fig. 1D). These findings suggest that the poorly metastatic PDX line HCI-002 evoked a cancer cell-independent mechanism that systemically inhibited metastatic breast cancer.

Next, we evaluated the nature of the immune microenvironment in lungs from mice bearing tumors from highly metastatic compared to poorly metastatic PDX lines (Fig. 1E). The 2 highly metastatic PDX lines (HCI-001 and HCI-010) induced a significant

Fig. 1. Monocyte recruitment in a nonmetastatic model. (A) Representative flow cytometry plots illustrating disseminated tumor cells (human CD298+ and mouse Lin− [lineage negative for CD31, CD45, and Ter119]) in lungs of HCI-001, HCI-010, and HCI-002 tumor-bearing mice. (B) Hematoxylin and eosin (H&E) staining of lungs show metastatic foci in HCI-001 and HCI-010 tumor-bearing mice, indicated with black arrows and dashed lines. (Scale bar, 50 μm.) (C) Schematic illustration of experimental approach. (D) Number of metastatic foci per lung lobe; HCI-001 (n = 8), HCI-001/HCI-002 (n = 8), HCI-002 (n = 5), mean ± SEM, 2 technical repeats. (E) Representative flow cytometry plots illustrate the gating of immune cells (CD45+), neutrophils (CD11b+Gr-1high), and monocytes/macrophages (CD11b+Gr-1low) in lungs of PDX tumor-bearing mice. (F) Frequency (percentage of CD45+) of lung monocytes in WT (n = 12), HCI-001 (n = 8), HCI-010 (n = 8), and HCI-002 (n = 14) tumor-bearing mice, mean ± SEM, >5 technical repeats. (G) Frequency (percentage of CD45+) of BrdU+ monocytes in bone marrow and lung after 2 (bone marrow [n = 6], lung [n = 5]), and 72 h (bone marrow [n = 4], lung [n = 4]) BrdU pulse, mean ± SEM, 3 technical repeats. (Mann–Whitney U test, *P < 0.05, **P < 0.01, ***P < 0.001).

Hagerling et al.

www.manaraa.com

increase in neutrophil (CD11b$^+$Gr-1^{high}) frequency in the lungs and a significant decrease in monocyte/neutrophil ratio compared to wild-type (WT) NOD/SCID mice (*SI Appendix*, Fig. S1 *B and C*), which supports previous findings showing that neutrophils can promote metastatic progression of breast cancer (15, 16). Interestingly, the lungs of mice bearing the poorly metastatic PDX line HCI-002 showed an increased frequency of monocytes/macrophages (CD11b$^+$Gr-1^{low}) (Fig. 1*F*). Analysis of BrdU incorporation at different time points in lungs and bone marrow showed that monocytes/macrophages (CD11b$^+$Gr-1^{low}, hereafter referred to as monocytes), most likely, was the end result of recruitment from the bone marrow rather than local proliferation of lung resident macrophages, further supporting a systemically mediated recruitment of monocytes. BrdU$^+$ monocytes in HCl-002 tumor-bearing mice were significantly lower in frequency in lung compared to bone marrow after 2 h of BrdU incubation and most probably accumulated in the lungs, as illustrated by a significant increase of BrdU$^+$ monocytes in lungs after 72 h of BrdU incubation, while there was no accumulation of BrdU$^+$ monocytes in bone marrow (Fig. 1*G*).

Taken together, our data indicate that the myeloid immune microenvironment in the metastatic niche can be different in the context of highly metastatic primary tumors compared to poorly metastatic primary tumors. Moreover, the PDX-derived data demonstrate that the myeloid immune response can be systemically and differentially activated in NOD/SCID mice and support the PDX model as a means of studying the role of myeloid cells in metastatic breast cancer.

Immune Effector Monocytes. To further characterize the recruited monocytes, we next asked whether C-C chemokine receptor type 2 (CCR2), a marker for circulating inflammatory monocytes (17), was present on monocytes infiltrating the lungs of HCI-002 tumor-bearing mice. Immunohistochemical (IHC) staining for CCR2 revealed clusters of CCR2$^+$ cells with a monocyte-type morphology in the lungs of the poorly metastatic PDX line HCI-002, but few in HCI-001 and HCI-010 tumor-bearing mice (Fig. 2*A*). By flow cytometry, we confirmed that mice transplanted with HCI-002 tumors had an increased infiltration of CCR2$^+$ monocytes into the lungs (Fig. 2 *B* and *C* and *SI Appendix*, Fig. S2 *A* and *B*). Of note, the infiltration of CCR2$^+$ monocytes to the mammary gland of wild-type mice and to the primary tumor of PDX-bearing mice did not differ (*SI Appendix*, Fig. S2C), hence tumor-derived CCL2 might primarily act on CCR2$^+$ monocytes in the bone marrow, initiating their recruitment to the lungs.

Our PDX-derived data revealed that the myeloid immune microenvironment in the metastatic niche can be different in the context of metastatic primary tumors compared to nonmetastatic primary tumors and suggested an antimetastatic role for CCR2$^+$ monocytes. To determine whether this correlation can also be observed in clinical samples, we evaluated pleural effusions from breast cancer patients for the presence of CCR2$^+$ cells by IHC. Intriguingly, pleural effusions with a large number of malignant cells largely lacked infiltrating CCR2$^+$ cells. In contrast, pleural effusions with a low number of malignant cells had abundant infiltration of CCR2$^+$ cells with monocyte-type morphology (Fig. 2 *D* and *E*). Taken together, the CCR2 staining on pleural effusions from breast cancer patients supported an antimetastatic role for CCR2$^+$ monocytes. They clearly demonstrate that the nature of the myeloid microenvironment at the metastatic site can be profoundly different between breast cancer patients and suggest that a high number of CCR2$^+$ cells might be correlated with lower metastatic burden.

Environmental cues, including tumor-derived factors, can reprogram myeloid cells at the transcriptional level and thereby dictate their phenotype (18). To expand our knowledge of how CCR2$^+$ monocytes in a nonmetastatic context can be reprogrammed and how they inhibit metastatic outgrowth, we compared CCR2$^+$ monocytes infiltrating the lungs of HCI-002 tumor-bearing mice

to CCR2$^+$ monocytes infiltrating the lungs of mice bearing the highly metastatic PDX line HCI-001 by RNA sequencing (RNAseq). Transcriptomic analysis of CCR2$^+$ monocytes from HCI-002 tumor-bearing mice revealed an up-regulation of genes associated with an immune effector response (e.g., *C1qc*, *Trpm4*, *Trim11*, *Pglyrp1*, *Ccl2*, *Il6*, *Ifit3*, and *Ifit2*), and gene ontology (GO) analysis revealed a pattern of enrichment in pathways related to tumoricidal capacity (e.g., response to IFNγ, response to tumor necrosis factor [TNF], and regulation of natural killer activation, as compared to CCR2$^+$ monocytes from HCI-001 tumor-bearing mice) (Fig. 2 *F* and *G*). We did not find any significant difference in natural killer (NK) cell infiltration in lungs or in peripheral blood between WT and any of the PDX-bearing mice (*SI Appendix*, Fig. S2 *D* and *E*).

Reprogramming into Tumoricidal Neutrophils. Previous studies have shown that IFNγ and TNFα can enhance the killing capacity of neutrophils, and that CCR2$^+$ monocytes augment the fungal killing capacity of neutrophils (19–21). While macrophages and neutrophils cooperate against microbial pathogens (22), less is known about their cooperation against cancer. Accordingly, we next asked if CCR2$^+$ monocytes, which produced both IFNγ and TNFα (*SI Appendix*, Fig. S2 *F* and *G*), cooperate with neutrophils to prevent metastatic breast cancer by inducing a tumoricidal neutrophil phenotype. To this end we used Ly6G$^+$ neutrophils and CCR2$^+$ monocytes from immunocompetent Bagg albino laboratory bred (BALB/c) mice. Indeed, WT BALB/c Ly6G$^+$ neutrophils and CCR2$^+$ monocytes in coculture had significantly enhanced tumoricidal capacity (Fig. 3*A*). Of note, CCR2$^-$ monocytes lacked tumoricidal capacity and did not enhance the tumoricidal capacity of neutrophils (*SI Appendix*, Fig. S3 *A* and *B*). While recombinant TNFα alone killed breast cancer cells, it did not significantly enhance the tumoricidal capacity of WT BALB/c Ly6G$^+$ neutrophils in vitro (Fig. 3*B*). In contrast, recombinant IFNγ alone did not exert any killing capacity but significantly enhanced the killing capacity of Ly6G$^+$ neutrophils (Fig. 3*B*). To elaborate further on the finding that CCR2$^+$ monocytes accumulating in the lungs of HCI-002 tumor-bearing mice, might enhance the tumoricidal capacity of neutrophils, we determined the killing capacity of lung-derived neutrophils from the PDX model. We sorted lung neutrophils from WT NOD/SCID mice and from NOD/SCID mice bearing either the highly or poorly metastatic PDX lines and compared their tumoricidal capacity in vitro. Intriguingly, only neutrophils derived from lungs of HCI-002 tumor-bearing mice, which are significantly infiltrated with CCR2$^+$ monocytes (Fig. 2 *A*–*C*), were able to kill breast cancer cells (Fig. 3*C*).

Since we did not detect a systemic increase of IFNγ or TNFα in the serum from HCI-002 tumor-bearing mice compared to HCI-001 tumor-bearing mice, we hypothesized that neutrophils might be reprogrammed into a tumoricidal phenotype locally in the lung metastatic niche. Moreover, conditioned medium (CM) from cultured CCR2$^+$ monocytes did not enhance the tumoricidal capacity of neutrophils (*SI Appendix*, Fig. S3B), supporting the idea that the reprogramming into a tumoricidal phenotype might be contact dependent and occurs locally at the metastatic site. To this end, we performed single-cell gene-expression analysis on peripheral blood- and lung-derived neutrophils taken from HCI-001 and HCI-002 tumor-bearing mice (Fig. 3*D* and *SI Appendix*, Fig. S4*A*). We compared 96 genes related to the immune system and relevant for the metastatic niche (*SI Appendix*, Table S2). Remarkably, principal component analysis (PCA) plots (Fig. 3*E*) and unsupervised hierarchical clustering of individual HCI-002 neutrophils showed that the majority of peripheral blood-derived neutrophils were distinct from lung-derived neutrophils, supporting the idea that neutrophils were reprogrammed locally in the lung microenvironment (Fig. 3*F* and *SI Appendix*, Fig. S4*B*). On the contrary, the majority of peripheral blood-derived HCI-001
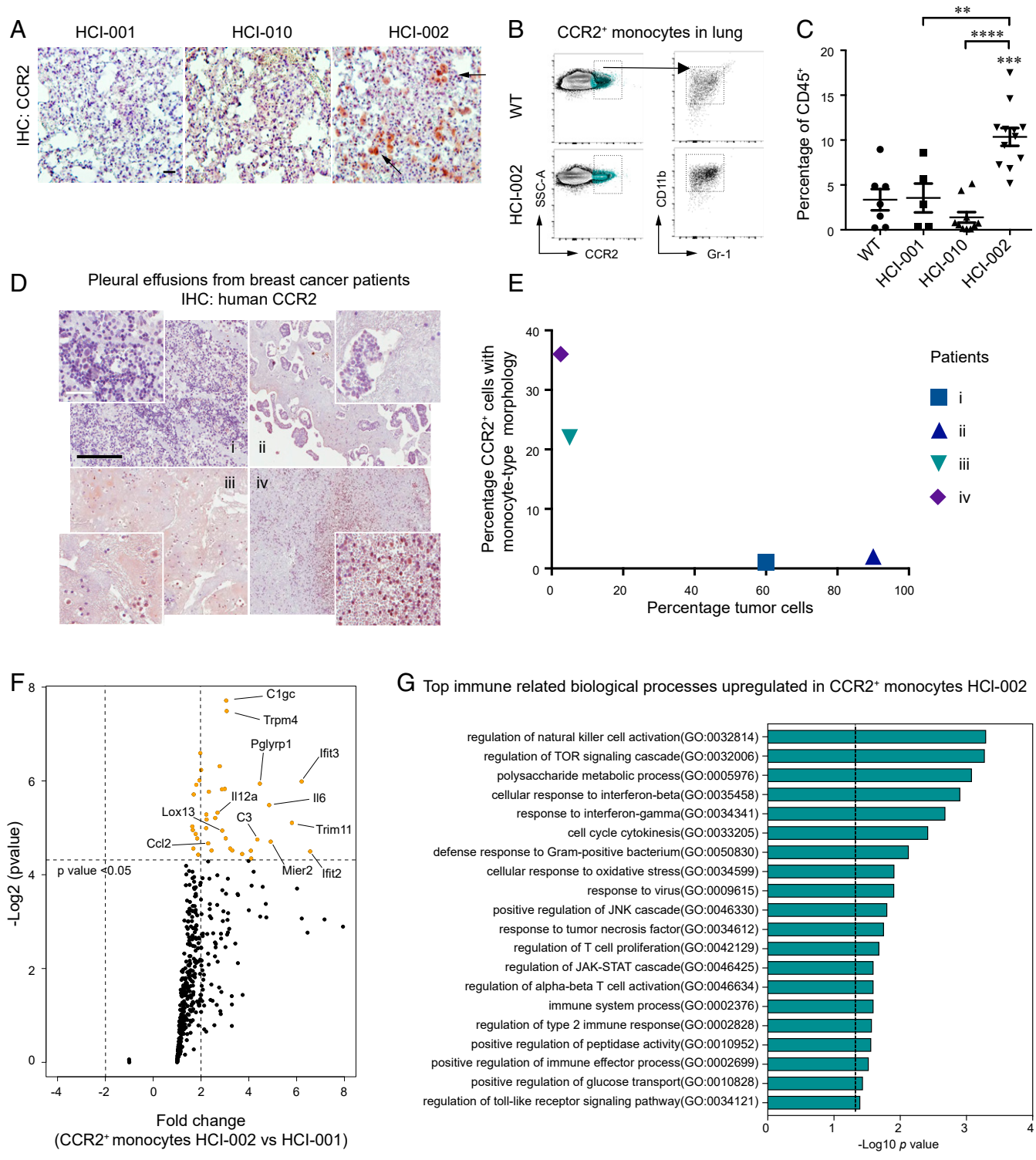
Hagerling et al.

www.manaraa.com

A HCI-001 HCI-010 HCI-002

IHC: CCR2

B CCR2⁺ monocytes in lung

WT

HCI-002

SSC-A

CCR2

CD11b

Gr-1

C

Percentage of CD45⁺

**

****

***

20

15

10

5

0

WT HCI-001 HCI-010 HCI-002

D Pleural effusions from breast cancer patients
IHC: human CCR2

i ii iii iv

E

Percentage CCR2⁺ cells with monocyte-type morphology

40

30

20

10

0

0 20 40 60 80 100

Percentage tumor cells

Patients

i

ii

iii

iv

F

-Log2 (pvalue)

8

6

4

2

0

C1gc

Trpm4

Pglyrp1

Ifit3

Il12a

Il6

Lox13

C3

Trim11

Ccl2

Mier2 Ifit2

p value <0.05

-4 -2 0 2 4 6 8

Fold change
(CCR2⁺ monocytes HCI-002 vs HCI-001)

G Top immune related biological processes upregulated in CCR2⁺ monocytes HCI-002

regulation of natural killer cell activation(GO:0032814)
regulation of TOR signaling cascade(GO:0032006)
polysaccharide metabolic process(GO:0005976)
cellular response to interferon-beta(GO:0035458)
response to interferon-gamma(GO:0034341)
cell cycle cytokinesis(GO:0033205)
defense response to Gram-positive bacterium(GO:0050830)
cellular response to oxidative stress(GO:0034599)
response to virus(GO:0009615)
positive regulation of JNK cascade(GO:0046330)
response to tumor necrosis factor(GO:0034612)
regulation of T cell proliferation(GO:0042129)
regulation of JAK-STAT cascade(GO:0046425)
regulation of alpha-beta T cell activation(GO:0046634)
immune system process(GO:0002376)
regulation of type 2 immune response(GO:0002828)
positive regulation of peptidase activity(GO:0010952)
positive regulation of immune effector process(GO:0002699)
positive regulation of glucose transport(GO:0010828)
regulation of toll-like receptor signaling pathway(GO:0034121)

0 1 2 3 4

-Log10 p value

Fig. 2. Immune effector CCR2⁺ monocytes. (*A*) Representative images of CCR2-stained PDX lungs. CCR2⁺ cells with a monocyte-type morphology (black arrow). (Scale bar, 50 μm.) (*B*) Representative flow cytometry plots of CCR2⁺ monocytes (CD11b⁺Gr-1^{low}) in lungs of PDX tumor-bearing mice. (*C*) Frequency (percentage of CD45⁺) of CCR2⁺ monocytes in lung of WT ($n = 7$), HCI-001 ($n = 5$), HCI-010 ($n = 10$), and HCI-002 tumor-bearing mice ($n = 12$), mean ± SEM (Mann–Whitney *U* test, **$P < 0.01$, ***$P < 0.001$, ****$P < 0.0001$). (*D*) Representative images of CCR2-stained pleural effusions from breast cancer patients. (*E*) Percentage of CCR2⁺ cells with monocyte morphology (brown) and tumor cells in pleural effusions from patient i–iv. (Scale bars, 50 μm [white] and 200 μm [black].) RNAseq data showing (*F*) volcano plot of immune effector genes (GO:0002252) and (*G*) GO analysis of biological processes upregulated in lung-derived CCR2⁺ monocytes from HCI-002 tumor-bearing mice ($n = 3$) compared to lung-derived CCR2⁺ monocytes from HCI-001 tumor-bearing mice ($n = 2$).

Hagerling et al.

MEDICAL SCIENCES

www.manaraa.com

Fig. 3. Reprogramming into tumoricidal neutrophils. (*A*) Tumoricidal capacity of Ly6G+ neutrophils in coculture with CCR2+ monocytes (control [*n* = 10], CCR2+ [*n* = 10], Ly6G+ [*n* = 22], CCR2+-Ly6G+ [*n* = 10]), mean ± SEM (Student's *t* test, *P* < 0.05, **P* < 0.01, ***P* < 0.001, ****P* < 0.0001, 4 technical replicates). (*B*) Tumoricidal capacity of Ly6G+ neutrophils (control [*n* = 12], Ly6G+ [*n* = 21]) together with recombinant CCL2 (CCL2 [*n* = 9], CCL2 -Ly6G+ [*n* = 9]), recombinant TNFα (TNFα [*n* = 12], TNFα -Ly6G+ [*n* = 21]) and recombinant IFNγ (IFNγ [*n* = 12], IFNγ -Ly6G+ [*n* = 21]), mean ± SEM (Student's *t* test, *P* < 0.05, **P* < 0.01, ***P* < 0.001, ****P* < 0.0001, 3 to 4 technical replicates). (*C*) Tumoricidal capacity of lung-derived neutrophils from WT and PDX-bearing mice (control [*n* = 18], WT [*n* = 4], HCI-001 [*n* = 3], HCI-002 [*n* = 5]), mean ± SEM (Mann–Whitney *U* test, *P* < 0.05, **P* < 0.01, 3 technical repeats). (*D*) Schematic illustration of experimental approach. (*E*) PCA plot showing a distinct population with peripheral blood (red) and lung-derived (green) neutrophils, from HCI-002-bearing mice, with some overlap. (*F*) Heatmap and dendrogram showing unsupervised hierarchical clustering of individual neutrophils from mice bearing HCI-002 tumors, for the genes that were significantly different between peripheral blood and lung-derived neutrophils (4 technical replicates).

neutrophils had similar gene-expression profiles to lung-derived HCI-001 neutrophils (*SI Appendix*, Fig. S4 *C and D*). Moreover, single-cell gene-expression analysis revealed that *ne* and *mmp9*, 2 genes associated with protumoral neutrophils (23), were negatively differentially expressed in HCI-002 compared to HCI-001 lung neutrophils (*SI Appendix*, Table S3).

Characterization of Tumoricidal Neutrophils. To characterize and elaborate further on the finding that lung neutrophils from HCI-002 tumor-bearing mice are antimetastatic and have enhanced tumoricidal capacity, we compared them to neutrophils from HCI-001 tumor-bearing mice by RNAseq. GO analysis on neutrophils purified from lungs of HCI-002 and HCI-001 tumor-bearing mice

Hagerling et al.

www.manaraa.com

confirmed that cellular pathways related to tumoricidal capacity (e.g., response to IFNγ, cell redox homeostasis, and inflammatory response) were up-regulated in neutrophils from the lungs of HCI-002 tumor-bearing mice (Fig. 4A). Moreover, RNAseq analysis revealed prominent differences between genes associated with immune effector response between the 2 groups of neutrophils. While *Lcp1* and *Atg5* were significantly down-regulated in HCI-002 compared to HCI-001 lung-derived neutrophils, *Ccl2*, *Il6*, and *Tmem173* were among a number of transcripts significantly up-regulated (Fig. 4B). Interestingly, TMEM173 (also known as STING and part of the cGAS-STING pathway recognizing cytosolic DNA) is a transmembrane protein located in the endoplasmic reticulum (ER), which improves vaccination against metastatic breast cancer and mediates antitumor immunity (involving lymphocytes and dendritic cells) upon recognition of tumor-derived DNA (24–28). However, whether neutrophils also have a part in STING-mediated antitumoral immune response is largely unexplored.

In support of these observations that suggest an antitumoral neutrophil phenotype, we found that breast cancer patients with high gene expression of *TMEM173*, had significantly lower recurrence rates and, importantly, recombinant IFNγ increased the gene expression of TMEM173 in neutrophils (Fig. 4 *C* and *D*), further supporting a role for TMEM173 in the IFNγ-induced killing capacity of neutrophils. Future studies would be warranted to determine that *TMEM173*, indeed, is expressed by human neutrophils and not by the tumor cells or other stromal cells and explore other mediators besides IFNγ that could up-regulate TMEM173 in neutrophils.

Validation in an Immunocompetent Model. To validate an antimetastatic role for CCR2⁺ monocytes and *Tmem173*^high^ neutrophils in an immunocompetent model, we exploited the basal-like murine mammary cancer cell line 4T1 (29). We orthotopically transplanted 4T1 cells into syngeneic immunocompetent WT and CCR2 knockout (KO) BALB/c mice to recapitulate tumor progression and spontaneous metastasis. The primary tumors grew faster in CCR2KO mice and half of the mice in this group had to be killed before experimental week 6 (Fig. 5 *A* and *B*). By experimental week 6 the tumor burden between WT mice and remaining CCR2KO mice did not differ, hence the increase in metastatic burden seen in CCR2KO mice (Fig. 5C) was independent of tumor size. Immunofluorescent (IF) staining for CCR2 and cleaved caspase-3, which recognizes apoptotic cells, showed CCR2⁺ cells, which were F480⁺ (*SI Appendix*, Fig. S5A), in close proximity to cleaved caspase-3-positive metastatic 4T1 cells in the lungs of WT mice (Fig. 5 *D* and *E*). Moreover, IF staining showed CCR2⁺ cells in near proximity to Ly6G⁺ cells (*SI Appendix*, Fig. S5B) and revealed dense infiltration of Ly6G⁺/TMEM173⁺ neutrophils only in the area where we had found dense infiltration of CCR2⁺ cells surrounding apoptotic metastatic 4T1 cancer cells in WT mice (Fig. 5 *D* and *F*).

Taken together, these data further support an antimetastatic role for CCR2⁺ monocytes and local reprogramming of neutrophils into a tumoricidal TMEM173⁺ phenotype. Moreover, they support local cooperation between CCR2⁺ immune effector monocytes and TMEM173⁺ neutrophils against metastatic breast cancer in the lung microenvironment.

Cytokine Profile in the PDX Model. To explore the underlying mechanism for primary tumor-induced myeloid cooperation and the difference in myeloid cell recruitment between PDX lines HCI-001, HCI-010, and HCI-002, we analyzed serum from PDX-bearing mice on human cytokine arrays and evaluated RNAseq data previously done on the xenografts (10). The highly metastatic PDX lines HCI-001 and HCI-010 had similar cytokine profiles, including expression of the potent neutrophil chemoattractant, chemokine (C-X-C motif) ligand 1 (CXCL1) (*SI Appendix*, Fig. S4 *A–C*). In contrast, the transcript for C-C motif

chemokine ligand 2 (CCL2) was differentially expressed in the HCI-002 xenograft, and CCL2 was detected by the human cytokine array only in serum from HCI-002 tumor-bearing mice, but not in the 2 other PDX lines (*SI Appendix*, Fig. S4 *A* and *B*). Intriguingly, further analysis of serum with the human cytokine 42-plex discovery assay revealed that CCL2 was the top cytokine differentially produced in HCI-002 compared to HCI-001 tumors (Fig. 6A). Importantly, CCL2 is a ligand for CCR2 and is important for the recruitment of CCR2⁺ monocytes (30). Significant for these studies, human CCL2 binds to murine CCR2 (31, 32). We further confirmed the difference in tumor-derived CCL2 with a human-specific ELISA for CCL2 in serum from PDX mice. CCL2 was produced at a considerably higher level by the PDX line HCI-002 (Fig. 6B).

Lower Recurrence Rate for CCL2^int/high Tumors. Our breast cancer PDX model with known differences in metastatic efficiency gave us a unique and clinically relevant opportunity to reveal a tumor-derived factor that can create an antimetastatic lung microenvironment, namely CCL2. To expand our understanding and clinically validate our PDX-derived data in human breast cancer, we stained a breast cancer TMA that included 406 primary tumor samples with at least 10 y follow-up (33) for CCL2 (Fig. 6C). Intriguingly, the patients with CCL2^low tumors, accounting for ~20% of the cases, had significantly higher recurrence rates (including local, regional, and distant recurrences), (Fig. 6D and *SI Appendix*, Table S2), and this was independent of breast cancer subtype (*SI Appendix*, Fig. S6 *A–C*). The majority of tumors, however, were CCL2^int/high and these patients had a much better prognosis (Fig. 6D and *SI Appendix*, Table S2). Worthy of note, we interrogated 39 microarray data of established breast cancer PDX lines, which are from patients with a poor prognosis (34). These data demonstrated that CCL2 had low expression in the majority of PDX lines, which further supports a nontumorigenic role for CCL2 (Fig. 6E).

Discussion

Previous studies generally have focused on identifying mechanisms that promote metastatic progression of breast cancer (4, 7). Here we took a somewhat contrary approach and inquired whether the fact that the majority of breast cancer patients, including those with tumors growing as rapidly as highly metastatic tumors, do not develop metastatic breast cancer might be due to their primary tumors evoking an antimetastatic myeloid immune response. We focused our investigation on myeloid cells, since myeloid cells are critical regulators of metastatic progression and the potential of targeting and modulating them therapeutically still remains largely unexplored. Here we uncovered a tumor-initiated myeloid cell-controlled pathway where immune effector monocytes and TMEM173⁺ neutrophils cooperate against metastatic breast cancer. Intriguingly, neutrophils become TMEM173⁺ in the lung microenvironment infiltrated with CCR2⁺ monocytes surrounding apoptotic metastatic breast cancer cells, supporting myeloid cooperation against metastatic breast cancer. Indeed, activation of the STING pathway with the agonist, 5,6-dimethylxanthenone-4-acetic acid (DMXAA) has been shown to induce recruitment and cooperation between T lymphocytes, monocytes, and neutrophils against breast cancer (35). Importantly, our PDX model was propagated in NOD/SCID mice, which lack functional T lymphocytes, which could imply that TMEM173-mediated antitumoral myeloid immune response might also function independent of T lymphocytes.

In our model, IFNγ up-regulated *Tmem173* and enhanced the tumoricidal capacity of neutrophils. In line with our findings, previous work has shown that IFNγ, and also TNF and CCL2, can enhance the killing capacity of neutrophils (19, 21, 24, 36). While we did not find any evidence that TNFα or CCL2 enhanced the killing capacity of neutrophils or recruitment of CCR2⁺
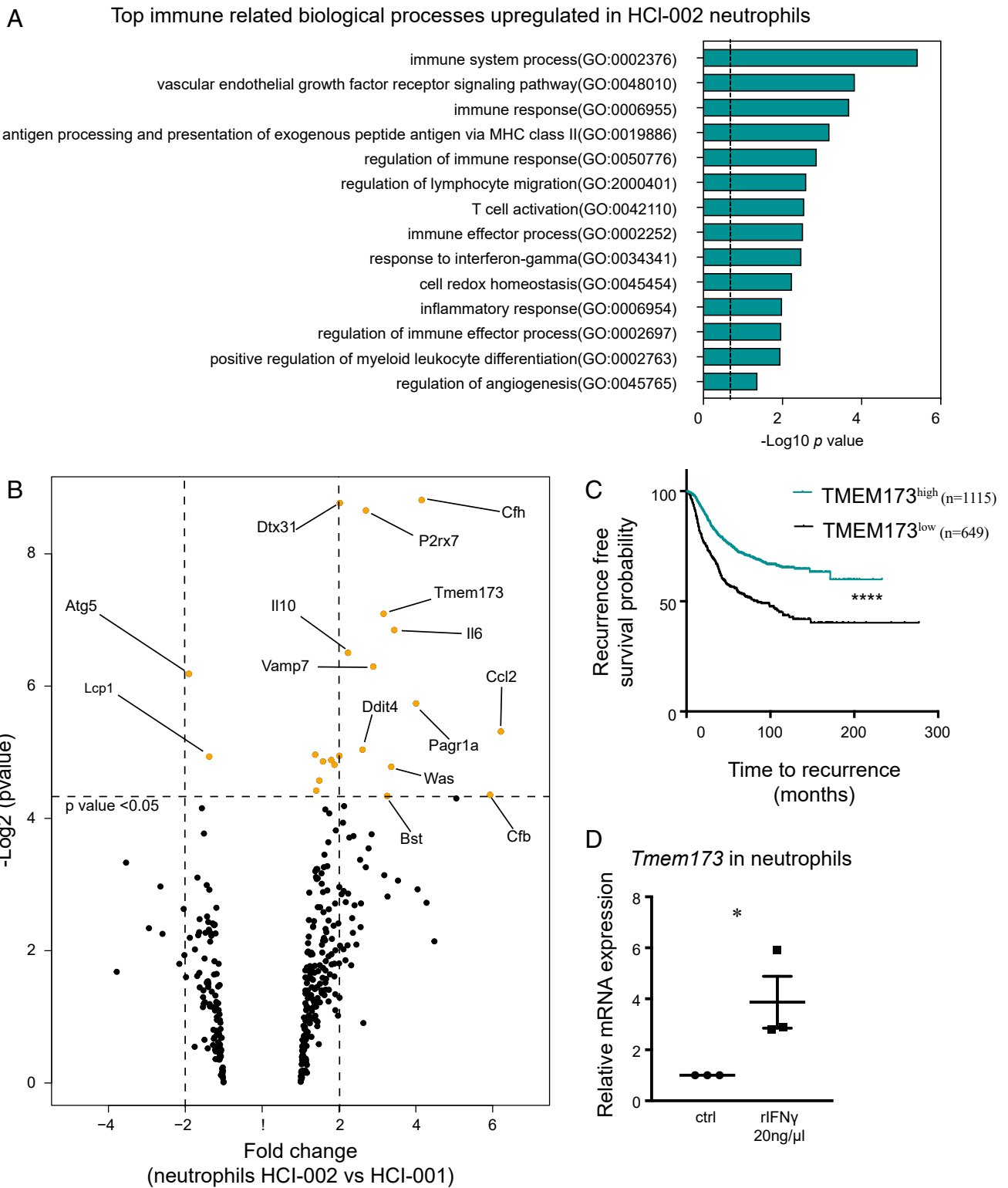
MEDICAL SCIENCES

www.manaraa.com

Fig. 4. Characterization of tumoricidal neutrophils. (*A*) GO analysis of biological processes up-regulated in lung-derived neutrophils from HCI-002 tumor-bearing mice (*n* = 3) compared to lung-derived neutrophils from HCI-001 tumor-bearing mice (*n* = 2). (*B*) Volcano plot of immune effector genes (GO:0002252) in lung-derived neutrophils from HCI-002 tumor-bearing mice (*n* = 3) compared to lung-derived neutrophils from HCI-001 tumor-bearing mice (*n* = 2). (*C*) Kaplan–Meier plots displaying recurrence-free survival of breast cancer patients with either low (black) or high (green) gene expression of *TMEM173* (Log-rank test, ****P < 0.0001). (*D*) Relative mRNA expression of *Tmem173* in control WT BALB/c peripheral blood Ly6G⁺ neutrophils and Ly6G⁺ neutrophils treated with 20 ng/μL recombinant IFNγ in OptiMEM medium for 16 h, mean ± SEM (Student's *t* test, *P < 0.05, 3 technical repeats).
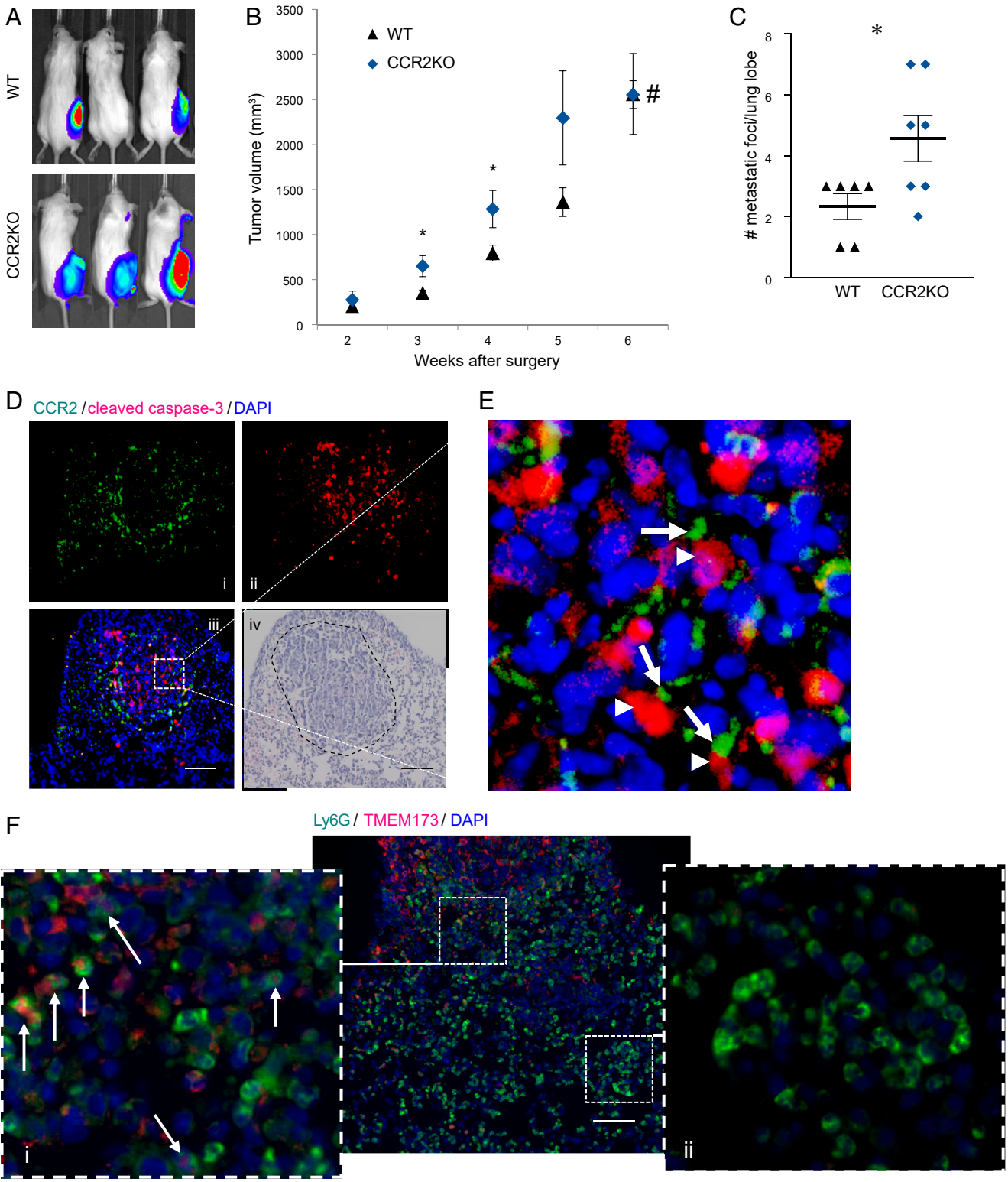
Fig. 5. Validation in an immunocompetent model. (*A*) In vivo imaging systems of WT and CCR2KO BALB/c mice 4 wk after orthotopically transplanted with 4T1 cancer cells. (*B*) Tumor growth kinetics in WT (*n* = 15) and CCR2KO mice (*n* = 10), mean ± SEM. #At 6 wk, 12 of WT mice were still in the experiment, while only 5 CCR2KO mice were left due to tumors growing to end point (∼20 to 25 mm in diameter) prior to 6 wk. (*C*) Number of spontaneous metastatic foci per lung lobe in WT (*n* = 12) and CCR2KO mice (*n* = 10), mean ± SEM (Student's *t* test, *P < 0.05). (*D*) Metastatic foci in WT lung stained for (*i*) CCR2 (green), (*ii*) cleaved caspase-3 (red), (*iii*) merge (DAPI [blue]), and (*iv*) H&E of the same lung section with a dashed line around the metastatic foci. (Scale bar, 50 μm.) (*E*) Magnification of metastatic foci in *D*, showing CCR2+ cells (green, indicated with white arrows) in intimate proximity with apoptotic cancer cells (red, indicated with white arrowheads). (*F*) Merged picture. Metastatic foci in WT BALB/c lung stained for Ly6G (green), TMEM173 (red), and DAPI (blue). (Scale bar, 50 μm.) (*i*) Magnification of Ly6G+/TMEM173+ cells indicated with white arrows within the metastatic foci. (*ii*) Magnification of Ly6G+/TMEM173− cells outside the metastatic foci.

Hagerling et al.

www.manaraa.com
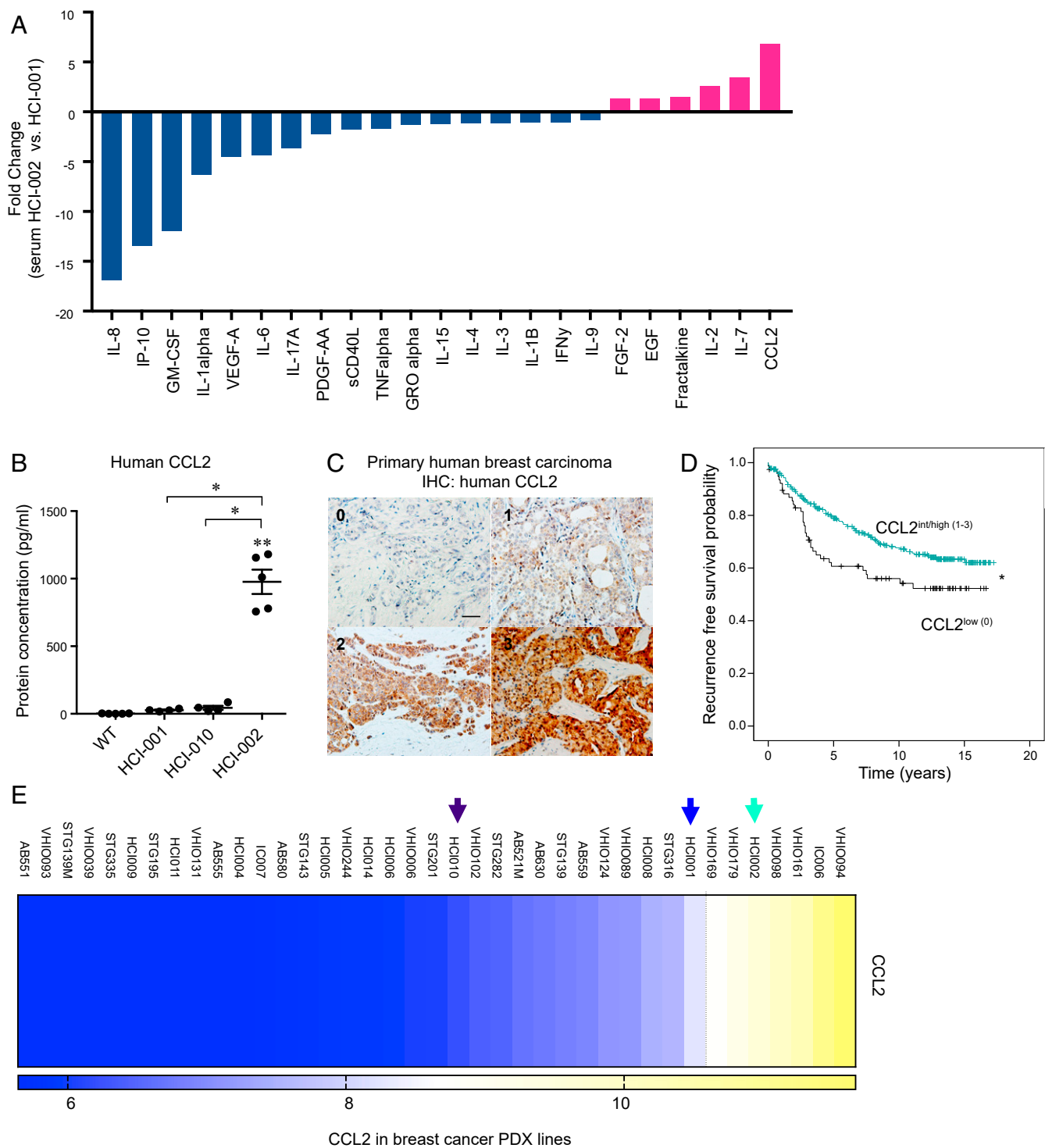
Fig. 6. Antimetastatic role of CCL2. (*A*) Human cytokines detected in serum from HCI-002 and HCI-001 tumor-bearing mice using human multiplex cytokine array. Cytokines not detected by the array are not shown. Data are expressed as fold change of the mean of 3 mice for each group. (*B*) Concentration of human CCL2 in serum from WT ($n = 5$), HCI-001 ($n = 4$), HCI-010 ($n = 4$), HCI-002-tumor-bearing mice ($n = 5$), mean ± SEM (Mann–Whitney *U* test, *$P < 0.05$, **$P < 0.01$). (*C*) Representative images of CCL2-stained primary human breast cancer tumors; score 0, score 1, score 2, and score 3. (Scale bar, 50 μm.) (*D*) Kaplan–Meier plots (Log-rank test) displaying recurrence-free survival according to CCL2$^{low\ (0)}$ and CCL2$^{int/high\ (1-3)}$ tumor-staining intensity in primary human breast cancer, (Log-rank test, *$P < 0.05$). (*E*) Analysis of CCL2 transcript expression in PDX samples reveals that the great majority of established breast cancer PDX lines are *CCL2^{low}*. Arrows indicate PDX lines HCI-001, HCI-010, and HCI-002.

neutrophils, IFNγ-producing CCR2$^+$ monocytes significantly infiltrated the lungs of mice transplanted with the poorly metastatic CCL2^{high} PDX line HCI-002 and only HCI-002 lung neutrophils, which were *Tmem173^{high}*, had tumoricidal capacity. The

above data concerning the role of IFNγ and up-regulation of Tmem173 and enhanced tumoricidal capacity, together with neutrophil-reprogramming occurring in the lung and the fact that neutrophils became TMEM173$^+$ only in the lung microenvironment

Hagerling et al.

www.manaraa.com

infiltrated with CCR2$^+$ monocytes, indicate a role for IFNγ-producing CCR2$^+$ monocytes and the enhanced tumoricidal capacity of TMEM173$^+$ neutrophils. However, whether stimulation with IFNγ and up-regulation of *Tmem173* is a prerequisite for conditioning into tumoricidal neutrophils is still unknown and will have to be determined by future studies.

The data concerning the role of CCR2$^+$ monocytes and its chemokine CCL2 for metastatic progression are contradictory. On the one hand, there are data, in line with our work, showing that CCR2$^+$ monocytes are cytotoxic (20) and antitumoral (37) and that CCL2 in breast cancer has an antimetastatic role (36, 38, 39). On the other hand, there are data showing that CCR2$^+$ monocytes and CCL2 are involved in promoting metastatic breast cancer (40–45). Notably, the great majority of prior studies showing that CCR2$^+$ monocytes and CCL2 promote metastatic progression, have injected breast cancer cells i.v. or intracardially into mice with no primary tumors, which does not capture the role of CCR2$^+$ monocytes and CCL2 in clinically relevant spontaneous metastatic progression of breast cancer. Importantly, we investigated the role of CCR2$^+$ monocytes and CCL2 in spontaneous metastasis, which more faithfully depicts clinical metastatic progression and our data emanated from PDX models that resemble the parental tumor histology and were established as reliable models harboring bona fide properties directly from breast cancer patients. Here we showed that CCR2$^+$ monocytes in a CCL2^{high} context acquired an immune effector profile and inhibited metastatic progression of breast cancer. Importantly, CCR2$^+$ monocytes in a CCL2^{low} context had a significantly different transcriptomic profile. Hence, the contradictory findings of CCR2$^+$ monocytes in breast cancer might partially be explained by the fact that the inflammatory milieu dictates their phenotype and, accordingly, the tumoral role of CCR2$^+$ monocytes. Indeed, the CCR2 receptor has other ligands besides CCL2 (46). Future studies are warranted to understand the potential role of other tumor-derived ligands responsible for recruitment of CCR2$^+$ monocytes and unravel other additional markers to better characterize subpopulations of CCR2$^+$ monocytes.

The clinical relevance of our PDX-derived data was confirmed with a large breast cancer TMA. Importantly, breast cancer patients with CCL2$^{int/high}$ tumors had a significantly lower recurrence rate. Our study analyzes the protein levels of CCL2 in breast cancer tumor cells, specifically, and correlates it to both clinicopathological features and recurrence. Our data are in line with a previous study showing that high CCL2 serum levels in breast cancer patients correlated with favorable prognostic variables (47). Other clinical papers, commonly cited when claiming that CCL2 correlates with decreased survival, either only determined that tumor cells express CCL2 (48), or correlated CCL2 with ER negativity, but did not provide any clinical outcome data (49). Indeed, we observed that CCL2 is more highly expressed in ER-negative and basal breast cancer, but importantly, breast cancer patients with CCL2$^{int/high}$ tumors within each breast cancer subtype more rarely had recurrence. Worthy of note, there are now therapeutic alternatives being developed aiming at targeting the CCL2/CCR2 axis in cancer patients (46). With our clinically validated data revealing an antimetastatic role for CCL2 and CCR2$^+$ monocytes in breast cancer, great caution should be taken before administrating drugs targeting the CCL2/CCR2 axis.

Taken together our study revealed one mechanism by which bone marrow-derived CCR2$^+$ immune effector monocytes, systemically recruited by tumor-derived CCL2, in cooperation with tumoricidal TMEM173$^+$ neutrophils prevent metastatic outgrowth of breast cancer (Fig. 7). It is, however unlikely that the CCL2/CCR2/TMEM173 axis is the only mechanism by which breast cancer tumors control metastatic progression. Moreover, the CCL2/CCR2/TMEM173 axis might be unique to the lung
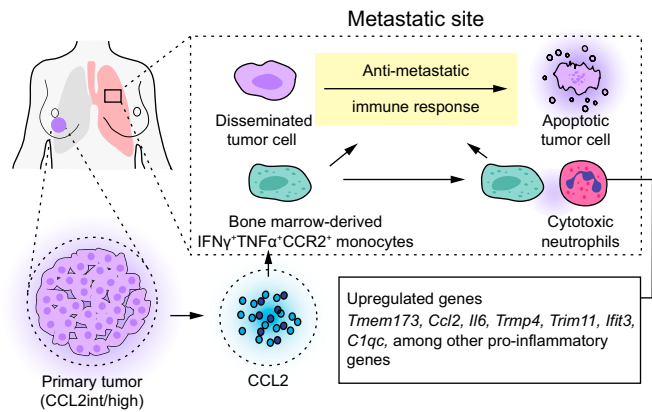

Fig. 7. A working model of a tumor-initiated, myeloid cell-controlled pathway that is antimetastatic. Tumor-derived CCL2 systemically recruits cytotoxic IFNγ- and TNFα-producing CCR2$^+$ immune effector monocytes from the bone marrow to the lungs. CCR2$^+$ monocytes in the lungs then reprogram and enhance the antitumoral capacity of neutrophils. While TNFα has a direct tumoricidal effect, IFNγ up-regulates *Tmem173* and enhances the killing capacity of neutrophils. CCR2$^+$ monocytes act in cooperation with tumoricidal *Tmem173*^{high} neutrophils locally in the lung microenvironment preventing metastatic outgrowth of breast cancer.

metastatic niche, since the metastatic efficiency to the bone marrow did not differ in our PDX model (metastatic efficiency to bone marrow: 14.3%, 26%, and 16% for HCI-001, HCI-010, and HCI-002, respectively) (11), suggesting that other mechanisms might control the bone metastatic niche. There were a number of other cytokines and chemokines that differed between metastatic and nonmetastatic tumors. Future studies, preferably including the wide array of established breast cancer PDX lines (34) would help elucidate which are significant regulators of metastasis and point to additional potential myeloid immunotherapeutic targets. Indeed, our data suggest that 20% of breast cancer patients, having CCL2^{low} tumors independent of breast cancer subtype, might benefit from the future development of cancer immunotherapies that activate and augment the function of antimetastatic immune effector monocytes and TMEM173$^+$ neutrophils.

Methods and Materials

Cell Lines and Animal Experiments. The syngeneic mammary cancer cell line 4T1 were obtained from the American Type Culture Collection (ATCC) or University California, San Francisco (UCSF) Cell Culture Facility and authenticated by short-tandem repeat profiling by ATCC. *Mycoplasma* contamination testing was performed routinely. The 4T1 cells were grown in standard conditions that can be found on the ATCC site. Lentiviral vector PLKO (Addgene 29783) (50) was transfected using a lipid-based method into 4T1 cells. Transfected cells were selected using puromycin (3 μg/mL) for 10 wk, reseeding 1:10 every 2 to 3 d. The stable 4T1 cells were then fluorescence-activated cell sorted by mCherry expression and screened for their luciferase activity using the Luciferase Assay System (Promega).

The generation and propagation of PDX tumors in NOD/SCID mice have been previously described (10, 11). NOD/SCID mice were purchased from The Jackson Laboratory. For spontaneous metastasis assays, 1×10^5 syngeneic 4T1 mammary cancer cells in 1:1 RPMI/Matrigel were injected orthotopically into the fourth mammary fat pad of 7-wk-old female BALB/c mice. Jason Rock, UCSF, San Francisco, CA, provided CCR2KO on BALB/c background (51). CCR2-sufficient BALB/c mice were either homozygous or heterozygous for CCR2. The growth kinetics of the tumors were measured by caliper weekly and the tumor volumes were calculated using the formula: V = $0.52 \times$ length $\times$ (width)^2. The UCSF Institutional Animal Care and Use Committee approved all animal experiments. Blinding was not possible.

Tissue Collection. Peripheral blood for serum collection was collected after cutting the right atrium. The peripheral blood was allowed to clot at room temperature for 30 min and then centrifuged. The supernatant (serum) was collected and stored at −80 °C. Next, peripheral blood was collected by

MEDICAL SCIENCES

injecting 10 mM EDTA in D-PBS through the left ventricle. The peripheral blood was mixed 1:1 with 2% dextran for sedimentation of red blood cells using standard methods. Supernatants were collected, centrifuged, and any remaining erythrocytes were lysed. Bone marrow was collected from femurs by flushing marrow with Hanks' salt solution using a 27-G needle followed by centrifugation and lysis of any remaining erythrocytes. Primary tumors and lungs were mechanically chopped and placed in collagenase medium for 45 min at 37 °C followed by centrifugation and DNase treatment. Samples were filtered through a 70-μm filter and any remaining erythrocytes were lysed. All samples were frozen in 90% serum and 10% DMSO and stored in liquid N_2.

Fluidigm Dynamic Array Experiments. Viable neutrophils (CD45$^+$Ly6G$^+$ cells) in peripheral blood or lungs of tumor-bearing mice were single-cell sorted into a 96-well plate. All of the experimental procedures hereafter have been described in detail elsewhere (11). In brief, single-cell gene-expression experiments were performed using Fluidigm's 96.96 qPCR DynamicArray microfluidic chips.

Statistics. All of the data are expressed as mean ± SEM. GraphPad Prism 7 was used for all statistical analysis. P values were generated using the nonparametric test, Mann–Whitney U test, when sample size was less than 20; otherwise and when distribution was parametric, the unpaired 2-sided Student's t test was used. $P < 0.05$ was considered significant.

For the breast cancer tissue microarray, Kaplan–Meier analysis and log rank tests were used to illustrate differences in recurrence-free survival (RFS) according to CCL2 expression. All statistical tests were 2-sided and $P \leq 0.05$ was considered significant. Calculations were performed with IBM SPSS Statistics version 24.0 (SPSS Inc). The Ethical Committee at Lund University and the UCSF Committee on Human Research approved the research using human samples.

1. F. Kamangar, G. M. Dores, W. F. Anderson, Patterns of cancer incidence, mortality, and prevalence across five continents: Defining priorities to reduce cancer disparities in different geographic regions of the world. *J. Clin. Oncol.* **24**, 2137–2150 (2006).
2. B. Weigelt, J. L. Peterse, L. J. van 't Veer, Breast cancer metastasis: Markers and models. *Nat. Rev. Cancer* **5**, 591–602 (2005).
3. H. Kennecke et al., Metastatic behavior of breast cancer subtypes. *J. Clin. Oncol.* **28**, 3271–3277 (2010).
4. S. S. McAllister, R. A. Weinberg, The tumour-induced systemic environment as a critical regulator of cancer progression and metastasis. *Nat. Cell Biol.* **16**, 717–727 (2014).
5. D. N. Khalil, E. L. Smith, R. J. Brentjens, J. D. Wolchok, The future of cancer treatment: Immunomodulation, CARs and combination immunotherapy. *Nat. Rev. Clin. Oncol.* **13**, 394 (2016).
6. C. Engblom, C. Pfirschke, M. J. Pittet, The role of myeloid cells in cancer therapies. *Nat. Rev. Cancer* **16**, 447–462 (2016).
7. T. Kitamura, B. Z. Qian, J. W. Pollard, Immune cell promotion of metastasis. *Nat. Rev. Immunol.* **15**, 73–86 (2015).
8. K. Moses, S. Brandau, Human neutrophils: Their role in cancer and relation to myeloid-derived suppressor cells. *Semin. Immunol.* **28**, 187–196 (2016).
9. D. I. Gabrilovich, S. Ostrand-Rosenberg, V. Bronte, Coordinated regulation of myeloid cells by tumours. *Nat. Rev. Immunol.* **12**, 253–268 (2012).
10. Y. S. DeRose et al., Patient-derived models of human breast cancer: Protocols for in vitro and in vivo applications in tumor biology and translational medicine. *Curr. Protoc. Pharmacol.* **60**, 14.23.1–14.23.43 (2013).
11. D. A. Lawson et al., Single-cell analysis reveals a stem-cell program in human metastatic breast cancer cells. *Nature* **526**, 131–135 (2015).
12. Y. S. DeRose et al., Tumor grafts derived from women with breast cancer authentically reflect tumor pathology, growth, metastasis and disease outcomes. *Nat. Med.* **17**, 1514–1520 (2011).
13. L. D. Shultz et al., Multiple defects in innate and adaptive immunologic function in NOD/LtSz-scid mice. *J. Immunol.* **154**, 180–191 (1995).
14. X. Hu et al., Induction of M2-like macrophages in recipient NOD-scid mice by allogeneic donor CD4(+)CD25(+) regulatory T cells. *Cell. Mol. Immunol.* **9**, 464–472 (2012).
15. S. K. Wculek, I. Malanchi, Neutrophils support lung colonization of metastasis-initiating breast cancer cells. *Nature* **528**, 413–417 (2015).
16. C. Hagerling, Z. Werb, Neutrophils: Critical components in experimental animal models of cancer. *Semin. Immunol.* **28**, 197–204 (2016).
17. S. Gordon, P. R. Taylor, Monocyte and macrophage heterogeneity. *Nat. Rev. Immunol.* **5**, 953–964 (2005).
18. R. Ostuni, F. Kratochvill, P. J. Murray, G. Natoli, Macrophages and cancer: From mechanisms to therapeutic implications. *Trends Immunol.* **36**, 229–239 (2015).
19. E. Comen et al., TNF is a key cytokine mediating neutrophil cytotoxic activity in breast cancer patients. *NPJ Breast Cancer* **2**:16009 (2016).
20. V. Espinosa et al., Inflammatory monocytes orchestrate innate antifungal immunity in the lung. *PLoS Pathog.* **10**, e1003940 (2014).
21. T. N. Ellis, B. L. Beaman, Interferon-gamma activation of polymorphonuclear neutrophil function. *Immunology* **112**, 2–12 (2004).
22. M. T. Silva, When two is better than one: Macrophages and neutrophils work in concert in innate immunity as complementary and cooperative partners of a myeloid phagocyte system. *J. Leukoc. Biol.* **87**, 93–106 (2010).
23. S. B. Coffelt, M. D. Wellenstein, K. E. de Visser, Neutrophils in cancer: Neutral no more. *Nat. Rev. Cancer* **16**, 431–446 (2016).
24. L. Corrales, T. F. Gajewski, Molecular pathways: Targeting the stimulator of interferon genes (STING) in the immunotherapy of cancer. *Clin. Cancer Res.* **21**:4774–4779 (2015).
25. D. Chandra et al., STING ligand c-di-GMP improves cancer vaccination against metastatic breast cancer. *Cancer Immunol. Res.* **2**, 901–910 (2014).
26. J. Klarquist et al., STING-mediated DNA sensing promotes antitumor and autoimmune responses to dying cells. *J. Immunol.* **193**, 6124–6134 (2014).
27. G. Pépin, M. P. Gantier, cGAS-STING activation in the tumor microenvironment and its role in cancer immunity. *Adv. Exp. Med. Biol.* **1024**, 175–194 (2017).
28. T. Li, Z. J. Chen, The cGAS-cGAMP-STING pathway connects DNA damage to inflammation, senescence, and cancer. *J. Exp. Med.* **215**, 1287–1299 (2018).
29. A. T. Egunsola et al., Growth, metastasis, and expression of CCL2 and CCL5 by murine mammary carcinomas are dependent upon Myd88. *Cell. Immunol.* **272**, 220–229 (2012).
30. S. L. Deshmane, S. Kremlev, S. Amini, B. E. Sawaya, Monocyte chemoattractant protein-1 (MCP-1): An overview. *J. Interferon Cytokine Res.* **29**:313–326 (2009).
31. Y. Yao, S. E. Tsirka, Mouse MCP1 C-terminus inhibits human MCP1-induced chemotaxis and BBB compromise. *J. Neurochem.* **118**, 215–223 (2011).
32. S. G. Sayyed et al., An orally active chemokine receptor CCR2 antagonist prevents glomerulosclerosis and renal failure in type 2 diabetes. *Kidney Int.* **80**, 68–78 (2011).
33. S. Borgquist et al., Oestrogen receptors alpha and beta show different associations to clinicopathological parameters and their co-expression might predict a better response to endocrine treatment in breast cancer. *J. Clin. Pathol.* **61**, 197–203 (2008).
34. A. Bruna et al., A biobank of breast cancer explants with preserved intra-tumor heterogeneity to screen anticancer compounds. *Cell* **167**:260–274.e22 (2016).
35. J. M. Weiss et al., The STING agonist DMXAA triggers a cooperation between T lymphocytes and myeloid cells that leads to tumor regression. *OncoImmunology* **6**, e1346765 (2017).
36. Z. Granot et al., Tumor entrained neutrophils inhibit seeding in the premetastatic lung. *Cancer Cell* **20**, 300–314 (2011).
37. K. B. Long et al., IFNγ and CCL2 cooperate to redirect tumor-infiltrating monocytes to degrade fibrosis and enhance chemotherapy efficacy in pancreatic carcinoma. *Cancer Discov.* **6**, 400–413 (2016).
38. M. Takahashi et al., Chemokine CCL2/MCP-1 negatively regulates metastasis in a highly bone marrow-metastatic mouse breast cancer model. *Clin. Exp. Metastasis* **26**, 817–828 (2009).
39. M. Li, D. A. Knight, L. A Snyder, M. J. Smyth, T. J. Stewart, A role for CCL2 in both tumor progression and immunosurveillance. *OncoImmunology* **2**, e25474 (2013).
40. L. Bonapace et al., Cessation of CCL2 inhibition accelerates breast cancer metastasis by promoting angiogenesis. *Nature* **515**, 130–133 (2014).
41. B. Z. Qian et al., CCL2 recruits inflammatory monocytes to facilitate breast-tumour metastasis. *Nature* **475**, 222–225 (2011).
42. X. Lu, Y. Kang, Chemokine (C-C motif) ligand 2 engages CCR2+ stromal cells of monocytic origin to promote breast cancer metastasis to lung and bone. *J. Biol. Chem.* **284**, 29087–29096 (2009).
43. M. B. Headley et al., Visualization of immediate immune responses to pioneer metastatic cells in the lung. *Nature* **531**, 513–517 (2016).
44. T. Hara et al., Control of metastatic niche formation by targeting APBA3/Mint3 in inflammatory monocytes. *Proc. Natl. Acad. Sci. U.S.A.* **114**, E4416–E4424 (2017).
45. T. Kitamura et al., CCL2-induced chemokine cascade promotes breast cancer metastasis by enhancing retention of metastasis-associated macrophages. *J. Exp. Med.* **212**, 1043–1059 (2015).
46. S. Y. Lim, A. E. Yuzhalin, A. N. Gordon-Weeks, R. J. Muschel, Targeting the CCL2-CCR2 signaling axis in cancer metastasis. *Oncotarget* **7**, 28697–28710 (2016).
47. Z. A. Dehqanzada et al., Correlations between serum monocyte chemotactic protein-1 levels, clinical prognostic factors, and HER-2/neu vaccine-related immunity in breast cancer patients. *Clin. Cancer Res.* **12**:478–486 (2006).
48. T. Valković, K. Lucin, M. Krstulja, R. Dobi-Babić, N. Jonjić, Expression of monocyte chemotactic protein-1 in human invasive ductal breast cancer. *Pathol. Res. Pract.* **194**, 335–340 (1998).
49. C. Chavey et al., Oestrogen receptor negative breast cancers exhibit high cytokine content. *Breast Cancer Res.* **9**, R15 (2007).
50. C. Levy et al., Intronic miR-211 assumes the tumor suppressive function of its host gene in melanoma. *Mol. Cell* **40**, 841–849 (2010).
51. A. J. Lechner et al., Recruited monocytes and type 2 immunity promote lung regeneration following Pneumonectomy. *Cell Stem Cell* **21**:120–134.e7 (2017).

www.manaraa.com